

Experimental Quantum Stochastic Walks Simulating Associative Memory of Hopfield Neural Networks

Hao Tang,^{1,2,3} Zhen Feng,^{1,3} Ying-Han Wang,^{1,4} Peng-Cheng Lai,^{1,4} Chao-Yue Wang,^{1,4} Zhuo-Yang Ye,^{1,4} Cheng-Kai Wang,^{1,4} Zi-Yu Shi,^{1,3} Tian-Yu Wang,¹ Yuan Chen,^{1,3,5} Jun Gao,^{1,3,5} and Xian-Min Jin^{1,2,3,*}


¹*School of Physics and Astronomy, Shanghai Jiao Tong University, 200240 Shanghai, China*

²*Institute of Natural Sciences, Shanghai Jiao Tong University, 200240 Shanghai, China*

³*Synergetic Innovation Center of Quantum Information and Quantum Physics, University of Science and Technology of China, Hefei, 230026 Anhui, China*

⁴*Zhiyuan Innovative Research Center, Shanghai Jiao Tong University, 200240 Shanghai, China*

⁵*Institute for Quantum Science and Engineering and Department of Physics, Southern University of Science and Technology, Shenzhen, 518055, China*

 (Received 19 October 2018; revised manuscript received 11 December 2018; published 7 February 2019)

With the increasing crossover between quantum information and machine learning, quantum simulation of neural networks has drawn unprecedentedly strong attention, especially for the simulation of associative memory in Hopfield neural networks due to their wide applications and relatively simple structures that allow easier mapping to the quantum regime. Quantum stochastic walk, a strikingly powerful tool to analyze quantum dynamics, has recently been proposed to simulate the firing pattern and associative memory with a dependence on the Hamming distance. We successfully map the theoretical scheme into a three-dimensional photonic quantum chip and realize quantum-stochastic-walk evolution through well-controlled detunings of the propagation constant. We demonstrate a good match rate of the associative memory between the experimental quantum scheme and the expected result for Hopfield neural networks. The ability of quantum simulation for an important feature of a neural network combined with the scalability of our approach through low-loss-integrated-chip and straightforward Hamiltonian engineering provides a primary but steady step toward photonic artificial-intelligence devices for optimization and computation tasks with greatly increased efficiencies.

DOI: [10.1103/PhysRevApplied.11.024020](https://doi.org/10.1103/PhysRevApplied.11.024020)

I. INTRODUCTION

The crossover between quantum information and machine learning has been an emerging field [1] to generate both quantum-enhanced machine-learning tasks [2–6] and the machine-learning-assisted quantum algorithms [7–10]. The former uses the quantum superposition to speed up the machine-learning performance, which was recently studied in tasks such as principal-component analysis [2] and use of support-vector machines [3–5]. The latter applies machine-learning techniques to quantum problems ranging from the phase transition in condensed-matter physics [7,8] to quantum-state classification [9,10] to increase the data-processing efficiency for complex quantum systems.

Among the various machine-learning techniques, artificial neural networks have drawn lots of attention due to their versatile use for deep learning [11–13] and

neuromorphic computing [14,15]. Similarly to neural networks in the human brain, artificial neural networks consist of neuronal structures, and include mechanisms for attractor dynamics, firing patterns, training rules, etc. A very neat and popular type of neural network is a Hopfield network [16,17], a single-layered and recurrent neural network with undirected connections between neurons. The signal transmission between neurons is always directed, from the synapse in one neuron to the dendrites in the other neuron, but the bidirectional connections between two neurons can still be realized by mutual receipt of signals from the other's synapse, as illustrated in Fig. 1(a). With flexible connections among neurons, a Hopfield neural network has a prominent feature, associative memory, which directly drives the network to form the firing pattern at the energy minima closest to the initial input pattern [Fig. 1(b)]. Such a content-addressable memory system can be widely applied to optimization, image processing [18,19], and even identification of genetic segments of RNA [20], where the distance between patterns can be quantified by the Hamming distance and the energy

*xianmin.jin@sjtu.edu.cn

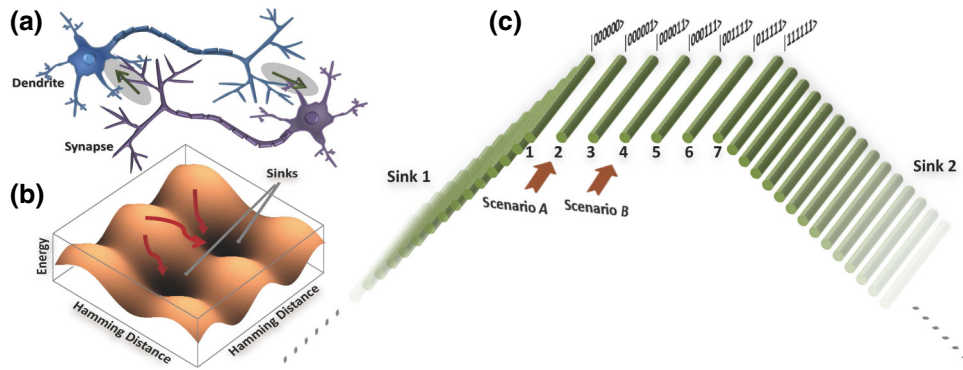


FIG. 1. The Hopfield network and the mapping to integrated photonics. (a) Bidirectional signal transmission between two neurons. The green arrows show the transmission from the synapse in one neuron to the dendrite in the other neuron. (b) The Hopfield network that memorizes the energy minima that are closest to the initial firing pattern in terms of the Hamming distance. (c) A seven-state network in the photonic waveguide array. Waveguides 1–7 represent the seven states, and the long array of waveguides on the sides represent the sink for state 1 and state 7, respectively. Two scenarios of initial patterns are considered, with the initial firing state being state 2 only in scenario A and being state 4 only in scenario B.

minima become the optimized task solution. Therefore, even though a Hopfield network is not as fancy as many trendy deep-learning networks, quantum simulations for the former are still appealing because it shows the important associative memory and its relatively simple structure allows easier mapping into the quantum regime, which can serve as building blocks for more-advanced quantum structures [20].

Quantum neural networks have hence been proposed and were hoped to fully comply with both neural-network mechanisms and quantum theory. However, this is confronted with a severe dilemma that the nonlinear activation functions inherently contradict the linear evolution in quantum theory [21]. Some recent theoretical proposals stick to complete neural networks using universal quantum gates [20,22,23], but their experimental realization could be too challenging at this stage, even for a single neuron, let alone a considerably large number of neurons that are required to make the neural network really work. On the other hand, some alternative approaches that simulate partial neural features (e.g., quantum associative memory [24–26]) have been more extensively studied in theory. A model of quantum stochastic walks, a mixture of quantum and classical walks [27], has been proposed to simulate the firing pattern and associative memory [28]. Although it is worth emphasizing that such simulation does not realize real quantum neurons, the mapping between neural networks and quantum stochastic walks has already been of great interest: there is a strong crossover between a representative neural feature and a very versatile quantum approach, thus bringing two separate fields together and greatly broadening the applications for each field. So far, this has been limited to theories only, but with the experimental advances of quantum walks [29–34] and quantum stochastic walks [35,36], its experimental demonstration becomes much more appealing and promising.

II. RESULTS

In this paper, we experimentally present the quantum stochastic walk in a three-dimensional (3D) photonic quantum chip and use it to demonstrate the feature of associative memory. In our setting, as shown in Fig. 1(c), we propose a seven-state network represented by an array of seven waveguides that sequentially correspond to the following states: $|000000\rangle$, $|000001\rangle$, $|000011\rangle$, $|000111\rangle$, $|001111\rangle$, $|011111\rangle$, and $|111111\rangle$. Each state differs from its neighboring state by a Hamming distance of 1; that is, only one different symbol in the same position of the two binary strings. In a mapping to waveguide arrays, the Hamming distance is equivalent to the count of waveguide spacings. For example, waveguide 1, which represents state 1 ($|000000\rangle$), has a Hamming distance of 6 (or six waveguide spacings) from waveguide 7 representing state 7 ($|111111\rangle$). The mutually evanescent coupling between neighboring photonic waveguides simulates the undirected connections in a Hopfield network. Now we make states 1 and states 7 two dynamic basins, or the “sink states,” by connecting to both waveguide 1 and waveguide 7 a long array of 50 auxiliary waveguides (see Appendix A for fabrication details). The spacing for adjacent auxiliary waveguides is much smaller than that for the seven state waveguides, yielding a much stronger coupling coefficient for the former, so photons will pass other states and evolve to the two sink states.

As suggested by Schuld *et al.* [28], the network evolution can be simulated by a quantum stochastic walk:

$$\frac{d\rho}{dt} = -(1 - \omega)i[H, \rho] + \omega \sum_{ij} \left(L_{ij} \rho L_{ij}^\dagger - \frac{1}{2} \{L_{ij}^\dagger L_{ij}, \rho\} \right), \quad (1)$$

where the first part on the right of the equation (containing $i[H, \rho]$) is the coherent and symmetric Hamiltonian term, and the second part (containing L_{ij} and L_{ij}^\dagger) is the classical Lindblad term, which causes diagonal and noncoherent environment noises in the open quantum system. In this model [28], the connections between sites are undirected, while addition of an extra directed site in the Lindblad term creates a sink of an energy minimum, and the noises from the Lindblad term assist and enhance the direct jump to those sinks.

A photonic model that realizes such quantum stochastic walks has been proposed [36]. It introduces quantitatively controllable diagonal decoherent terms into a photonic quantum system, and was demonstrated for a “maze”-escaping problem [36]. This method, which can be quite useful for simulating many problems in open quantum systems, had never been used in experiments since its invention. We manage to realize the experimental implementation once again, and apply it to an entirely new field, the simulation of a machine-learning feature.

In the photonic model, the diagonal and noncoherent noise can be created effectively by control of $\Delta\beta$, which is the detuning of the propagation constant in the diagonal term of the Hamiltonian matrix, while the long array of auxiliary waveguides can be used to create the sinks. In light of this $\Delta\beta$ model, we randomly pick $\Delta\beta$ from the uniform distribution of a certain amplitude, $\Delta\beta_A$. We fabricate the waveguide structure using femtosecond-laser direct writing and realize $\Delta\beta$ by adjusting the writing speed (see Appendix B for more details). We set a few $\Delta\beta_A$ values in different samples of the same array structure to vary the contribution of classical walk, since it was qualitatively demonstrated that a higher detuning amplitude of the propagation constant corresponds to a larger portion of the Lindblad terms in the quantum stochastic walk [36].

We now consider two representative scenarios of initial patterns, where the initial firing state is state 2 only in scenario A and state 4 only in scenario B. The two scenarios differ in their Hamming distance between the initial state and the sink states; that is, state 2 is closer to state 1 than to state 7, whereas state 4 has an equal Hamming distance to states 1 and 7. We inject the 780-nm vertically polarized laser beam into waveguides 2 and 4 to simulate scenarios A and B, respectively. We measure the evolution patterns using a charge-coupled-device (CCD) camera, with an example shown in Fig. 2, and calculate the ratio of the light intensity at sinks 1 and 2.

It was theoretically proven by both the Hopfield-neural-network model and the quantum-stochastic-walk model [28] that the walk always fully evolves to the sink state closest to the initial state in terms of the Hamming distance, and if there are two sink states of equal Hamming distance to the initial state, the walk will end up with equal probabilities at the two sink states. Most firing patterns can be classified into either of these two representative

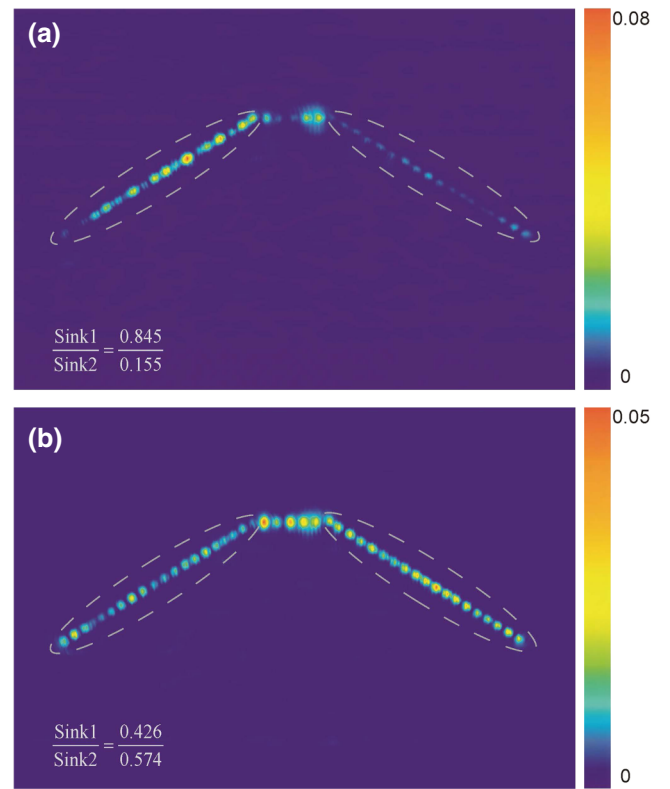


FIG. 2. Experimental evolution patterns. An experimental evolution pattern (a) for scenario A, with initial photon injection in state 2 and (b) for scenario B with initial photon injection in state 4. Both are from one sample with $\Delta\beta_A$ of 0.4 mm^{-1} . For each scenario, the dashed ellipses on the left and right sides correspond to sink 1 and sink 2, respectively, and the inserted data show the ratio of the light intensity in sink 1 to that in sink 2.

scenarios. In experiments, the probability distribution is reflected by the light intensity, and the results obtained agree with theory well. To quantitatively evaluate the performance, we propose that if the light intensity in sink state 1 is more than 2 times that in sink state 7 for scenario A, within certain experimental tolerance, the walk still has a clear preference for sink state 1 indicating the simulation of associative memory for scenario A is correct; for scenario B, we regard the simulation is correct if the light-intensity ratio stays between 40:60 and 60:40, which suggests a roughly balanced distribution. The values shown in Figs. 2(a) and 2(b) both indicate a correct simulation result.

We investigate the match rate of associative memory, as shown in Fig. 3. For both scenario A [Fig. 3(a)] and scenario B [Fig. 3(b)], we prepare 20 samples and analyze their light-intensity ratio from the measured patterns. Among the 20 samples we prepared, the configurations of the waveguide structure are identical but the $\Delta\beta$ values are different: there are four groups of $\Delta\beta_A$ values ($0.1, 0.2, 0.3,$ and 0.4 mm^{-1} , corresponding to groups A, B, C, and D, respectively), and each group includes five samples, which

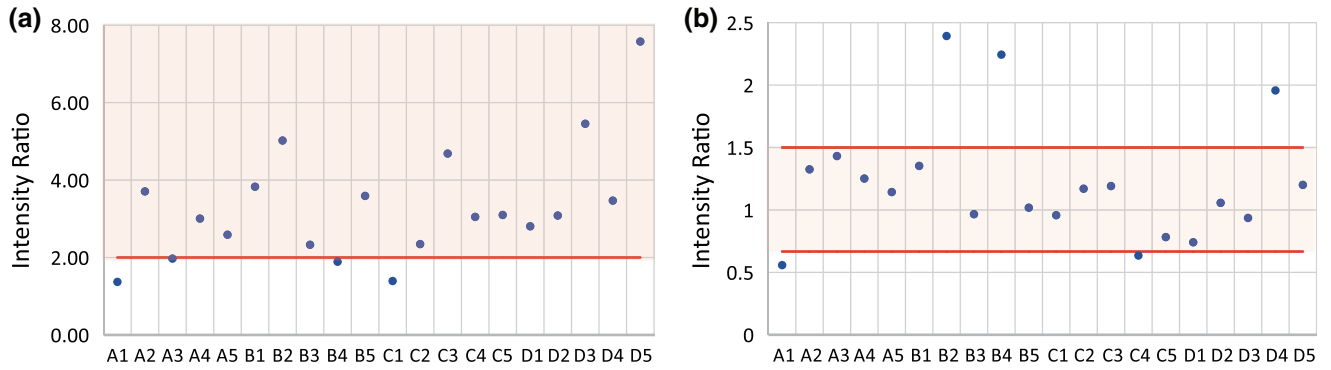


FIG. 3. The match rate for associative memory. The experimentally characterized light-intensity ratio of sink 1 and sink 2 for scenario A (a) and scenario B (b) for all 20 samples. The shadowed areas show the criteria of the correct simulation of associative memory for each scenario. The match rate for associative memory can be counted as the number of dots in the shadowed area to the total number of dots expressed as a percentage in each scenario.

have various random $\Delta\beta$ values but the same $\Delta\beta_A$ value. The dots in the shadowed range are those that show the correct simulation result, while the dots outside the range do not match our tight criteria, so we can assume that scenarios A and B have a match rate of the associative memory of 80% and 75%, respectively. The quantum stochastic walk on the photonic waveguide system thus demonstrates positive results for simulation of the associative-memory effect that is consistent with the theory [28].

From Fig. 3, the match rate does not show clear differences among groups of different $\Delta\beta_A$ amplitudes, which suggests a robust simulation of associative memory insensitive to the parameter of the quantum model. Additionally,

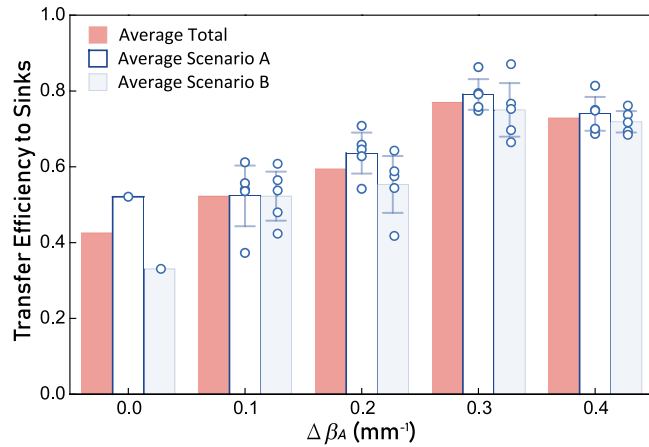


FIG. 4. The transfer efficiencies. The experimental transfer efficiencies to the sink states for samples with different $\Delta\beta_A$ in (a) scenario A and (b) scenario B. The small circles represent the individual results for each sample. The columns show the average for each group of the same $\Delta\beta_A$, and the corresponding error bars are calculated by the standard variance of the five individual results within each group. “Average Total” stands for the average value for all results from both scenario A and scenario B in the same group of $\Delta\beta_A$.

the change of $\Delta\beta_A$ has some other effects. As predicted in a theoretical paper [28], the proportion of the classical term in the quantum stochastic walk influences the transfer efficiency at the same evolution time. Correspondingly, we measure the ratio of the light intensity in sink states 1 and 7 to the total light intensity as the transfer efficiency to the sink states, and plot the transfer efficiency for samples of different $\Delta\beta_A$ in Fig. 4. For both scenario A and scenario B, the increase of $\Delta\beta_A$ clearly enhances the transport efficiency compared with the pure quantum walk, where $\Delta\beta_A$ equals zero. A slight drop of the transport efficiency when $\Delta\beta_A$ further increases to 0.4 mm^{-1} is consistent with the theoretical prediction that an optimal transfer efficiency exists at a certain classical amount of the walk. From the feature of the enhanced transfer efficiencies over pure quantum walks, we verify the positive role of classical terms in speeding up the formation of the associative memory in quantum stochastic walks.

III. CONCLUSION

Through this work, we present an attempt to experimentally simulate the associative memory of Hopfield networks using quantum stochastic walks on photonic waveguide arrays. The simulation does not realize full features of neurons, but focuses on a most-important feature of a Hopfield network, the associative memory. Just like a Hopfield network “memorizes” the dynamic basin that is close to the initial pattern in terms of the Hamming distance, we use the quantum stochastic walk of photons to “memorize” the correct sinks dependent on the waveguide spacing. We have a faithful implementation of the theoretical proposal by demonstrating the theoretically proposed two different and very representative types of firing patterns that most scenarios can be classified into. Both the theoretical proposal and our experimental results suggest a modest speedup through the approach of quantum stochastic walk. Even though the speedup is not extremely high,

we manage to set a real step forward toward its experimental demonstration, and this could serve as a building block for future quantum devices.

It is further inspiring to see the scalability of our approach for this work. The theoretical proposal itself has scaling advantages. It uses a very plain mapping into the quantum stochastic walks, which, even for very large evolution spaces, can be straightforwardly implemented in photonic systems. A concern is whether a larger scale in experiments would cause losses to destroy the originally modest quantum-speedup advantages, considering that error correction is critical for universal quantum computing, and only limited scales have been reported for some approaches using phase shifters [37–39] to construct a designed unitary matrix because of stringent fabrication requirements and a polynomially increasing number of phase shifters when the scale increases. On the other hand, our approach is to flexibly construct the Hamiltonian matrix that contains the coupling information through our defining the waveguide structure directly. The scalability for such a scheme could benefit from the larger-scale and lower-loss evolution system that can be straightforwardly laid out on integrated photonic chips, and the flexible and precise setting of coupling coefficients through curvature, space control, etc. These allow potential feasibility for wider associative memories in more-complex firing patterns, and a scalable solution to another task, experimental quantum fast hitting, was recently demonstrated [40]. In future, more tasks will be mapped into the Hamiltonian matrix on a photonic quantum chip with use of such an analog-quantum-computing approach. Our attempt as an elementary example brings opens up many possibilities for scalable analog-quantum-computing applications worthy of further exploration.

ACKNOWLEDGMENTS

The authors thank Roberto Osellame and Jian-Wei Pan for helpful discussions. This work was supported by the National Key R&D Program of China (Grant No. 2017YFA0303700), the National Natural Science Foundation of China (Grants No. 61734005, No. 11761141014, and No. 11690033), the Science and Technology Commission of Shanghai Municipality (Grants No. 15QA1402200, No. 16JC1400405, and No. 17JC1400403), the Shanghai Municipal Education Commission (Grants No. 16SG09 and No. 2017-01-07-00-02-E00049), and the Zhiyuan Scholar Program (Grants No. ZIRC2016-01 and No. ZIRC2017-05). X.-M.J. acknowledges support from the National Young 1000 Talents Plan.

APPENDIX A: WAVEGUIDE FABRICATION

To introduce the classical term of the quantum stochastic walk in the seven-waveguide array, we vary ΔV 40 times in the 8-cm-long evolution length of each waveguide. In other

words, ΔV in each segment of 2 mm is constant, but all of the random ΔV values in 280 segments (each of the seven waveguides has 40 segments) follow a uniform distribution with a given ΔV amplitude. All the waveguides are fabricated with the femtosecond-laser direct-writing technique [41–43]. We steer light from a 513-nm femtosecond laser (up-converted from a pump laser of 10 W, 1026 nm, 290-fs pulse duration, 1-MHz repetition rate) into a spatial light modulator to shape the laser pulse in time and spatial domains. We then focus the pulse onto a pure borosilicate substrate with a $\times 50$ objective lens (numerical aperture 0.55). Power and spatial-light-modulation compensation are performed to help ensure the waveguide uniformity [43].

In terms of the array arrangement, we originally set it in the two-dimensional planar form (i.e., the sink waveguides and the major waveguides are at the same depth). We cannot fine-tune the characterization as there is always some photonic evolution pattern when the injected light is moved horizontally and even not focused onto the input waveguide, perhaps due to the scattering of the injected light into other waveguides at the same depth. We then set the array in the current 3D form, and we easily locate the precise light distribution pattern. This suggests some advantage of the 3D layout.

APPENDIX B: $\Delta\beta$ APPROACH

We measure $\Delta\beta$ using the directional-coupler approach. One of the waveguides is written with a base speed $V_0 = 5$ mm/s, and the other waveguide is written with a different speed V ($V - V_0 = \Delta V$) that will lead to a detuned propagation constant $\Delta\beta$ on the waveguide. In the detuned directional coupler, the effective coupling coefficient C_{eff} can be obtained by use of the same coupling-mode method as for the normal directional coupler [44], but C_{eff} contains the detuning effect from $\Delta\beta$ through the equation [45] $C_{\text{eff}} = \sqrt{(\Delta\beta/2)^2 + C^2}$, where C is the coupling coefficient for the normal directional coupler. Therefore, $\Delta\beta$ can be calculated when C_{eff} and C are both characterized. We then plot $\Delta\beta$ (unit of per millimeter) against ΔV (unit of millimeters per second) and fit it linearly: $\Delta\beta = 0.20 \times \Delta V$. Knowing this, we can randomly generate $\Delta\beta$ of 0.01–0.4 mm^{-1} by varying ΔV between 0.5 and 20 mm/s.

-
- [1] J. Biamonte, P. Wittek, N. Pancotti, P. Rebentrost, N. Wiebe, and S. Lloyd, Quantum machine learning, *Nature* **549**, 195 (2017).
 - [2] S. Lloyd, M. Mohseni, and P. Rebentrost, Quantum principal component analysis, *Nat. Phys.* **10**, 631 (2014).
 - [3] P. Rebentrost, M. Mohseni, and S. Lloyd, Quantum Support Vector Machine for Big Data Classification, *Phys. Rev. Lett.* **113**, 130503 (2014).

- [4] X.-D. Cai, D. Wu, Z.-E. Su, M.-C. Chen, X.-L. Wang, L. Li, N.-L. Liu, C.-Y. Lu, and J.-W. Pan, Entanglement-Based Machine Learning on a Quantum Computer, *Phys. Rev. Lett.* **114**, 110504 (2015).
- [5] Z. Li, X. Liu, N. Xu, and J.-F. Du, Experimental Realization of a Quantum Support Vector Machine, *Phys. Rev. Lett.* **114**, 140504 (2015).
- [6] N. Spagnolo, E. Maiorino, C. Vitelli, M. Bentivegna, A. Crespi, R. Ramponi, P. Mataloni, R. Osellame, and F. Sciarrino, Learning an unknown transformation via a genetic approach, *Sci. Rep.* **7**, 14316 (2017).
- [7] J. Carrasquilla, and R. G. Melko, Machine learning phases of matter, *Nat. Phys.* **13**, 431 (2017).
- [8] E. P. L. van Nieuwenburg, Y.-H. Liu, and S. D. Huber, Learning phase transitions by confusion, *Nat. Phys.* **13**, 435 (2017).
- [9] J. Gao, L. F. Qiao, Z. Q. Jiao, Y. C. Ma, C. Q. Hu, R. J. Ren, A. L. Yang, H. Tang, M. H. Yung, and X. M. Jin, Experimental Machine Learning of Quantum States, *Phys. Rev. Lett.* **120**, 240501 (2018).
- [10] A separability-entanglement classifier via machine learning, *Phys. Rev. A* **98**, 012315 (2018).
- [11] Y. LeCun, Y. Bengio, and G. Hinton, Deep learning, *Nature* **521**, 436 (2015).
- [12] D. Silver *et al.*, Mastering the game of go with deep neural networks and tree search, *Nature* **529**, 484 (2016).
- [13] V. Mnih, K. Kavukcuoglu, D. Silver, A. A. Rusu, J. Veness, M. G. Bellemare, A. Graves, M. Riedmiller, A. K. Fidjeland, G. Ostrovski, S. Beattie, C. Sadik, A. Petersen, I. Antonoglou, H. King, D. Kumaran, D. Wierstra, S. Legg, and D. Hassabis, Human-level control through deep reinforcement learning, *Nature* **518**, 529 (2015).
- [14] P. A. Merolla *et al.*, A million spiking-neuron integrated circuit with a scalable communication network and interface, *Science* **345**, 668 (2014).
- [15] Y. C. Shen, N. C. Harris, S. Skirlo, M. Prabhu, T. Baehr-Hones, M. Hochberg, X. Sun, S. J. Zhao, H. Larochelle, D. Englund, and S. Soljačić, Deep learning with coherent nanophotonic circuits, *Nat. Photonics* **11**, 441 (2017).
- [16] J. J. Hopfield, Neural networks and physical systems with emergent collective computational abilities, *Proc. Natl. Acad. Sci.* **79**, 2554 (1982).
- [17] J. J. Hopfield, and D. W. Tank, Computing with neural circuits: A model, *Science* **233**, 625 (1986).
- [18] A. J. Tatem, H. G. Lewis, P. M. Atkinson, and M. S. Nixon, Super-resolution target identification from remotely sensed images using a Hopfield neural network, *IEEE Trans. Geosci. Remote Sens.* **39**, 781 (2001).
- [19] Y. Zhu and H. Yan, Computerized tumor boundary detection using a Hopfield neural network, *IEEE Trans. Med. Imaging* **16**, 55 (1997).
- [20] P. Rebentrost, T. R. Bromley, C. Weedbrook, and S. Lloyd, Quantum Hopfield neural network, *Phys. Rev. A* **98**, 042308 (2018).
- [21] M. Schuld, I. Sinayskiy, and F. Petruccione, The quest for a quantum neural network, *Quantum Inf. Process.* **13**, 2567 (2014).
- [22] Y. D. Cao, G. G. Guerreschi, and A. Aspuru-Guzik, Quantum neuron: An elementary building block for machine learning on quantum computers. arxiv:1605.04220 (2017).
- [23] K. H. Wan, O. Dahlsten, H. Kristjánsson, R. Gardner, and M. S. Kim, Quantum generalisation of feedforward neural networks, *npj Quant. Info.* **3**, 36 (2017).
- [24] D. Ventura, and T. Martinez, Quantum associative memory, *Info. Sci.* **124**, 273 (2000).
- [25] C. A. Trugenberger, Probabilistic Quantum Memories, *Phys. Rev. Lett.* **87**, 067901 (2001).
- [26] M. C. Diamantini and C. A. Trugenberger, High-capacity quantum associative memories, *J. Appl. Math. Phys.* **4**, 2079 (2015).
- [27] J. D. Whitfield, C. A. Rodríguez-Rosario, and A. Aspuru-Guzik, Quantum stochastic walks: A generalization of classical random walks and quantum walks, *Phys. Rev. A* **81**, 022323 (2010).
- [28] M. Schuld, I. Sinayskiy, and F. Petruccione, Quantum walks on graphs representing the firing patterns of a quantum neural network, *Phys. Rev. A* **89**, 032333 (2014).
- [29] J. Du, H. Li, X. Xu, M. Shi, J. Wu, X. Zhou, and R. Han, Experimental implementation of the quantum random-walk algorithm, *Phys. Rev. A* **67**, 042316 (2003).
- [30] H. Schmitz, R. Matjeschk, C. Schneider, J. Glueckert, M. Enderlein, T. Huber, and T. Schaetz, Quantum Walk of a Trapped Ion in Phase Space, *Phys. Rev. Lett.* **103**, 090504 (2009).
- [31] H. B. Perets, Y. Lahini, F. Pozzi, M. Sorel, R. Morandotti, and Y. Silberberg, Realization of Quantum Walks with Negligible Decoherence in Waveguide Lattices, *Phys. Rev. Lett.* **100**, 170506 (2008).
- [32] A. Schreiber, A. Gábris, P. P. Rohde, K. Laiho, M. Stefaňák, V. Potoček, C. Hamilton, I. Jex, and C. Silberhorn, A 2D quantum walk simulation of two-particle dynamics, *Science* **336**, 55 (2012).
- [33] Y. C. Jeong, C. Di Franco, H. T. Lim, M. S. Kim, and Y. H. Kim, Experimental realization of a delayed-choice quantum walk, *Nat. Commun.* **4**, 2471 (2013).
- [34] H. Tang, X. F. Lin, Z. Feng, J. Y. Chen, J. Gao, K. Sun, C. Y. Wang, P. C. Lai, X. Y. Xu, Y. Wang, L. F. Qiao, A. L. Yang, and X. M. Jin, Experimental two-dimensional quantum walk on a photonic chip, *Sci. Adv.* **4**, eaat3174 (2018).
- [35] D. N. Biggerstaff, R. Heilmann, A. A. Zecevik, M. Gräfe, M. A. Broome, A. Fedrizzi, S. Nolte, A. Szameit, A. G. White, and I. Kassal, Enhancing quantum transport in a photonic network using controllable decoherence, *Nat. Commun.* **7**, 11282 (2016).
- [36] F. Caruso, A. Crespi, A. G. Ciriolo, F. Sciarrino, and R. Osellame, Fast escape of a quantum walker from an integrated photonic maze, *Nat. Commun.* **7**, 11682 (2016).
- [37] N. C. Harris, G. R. Steinbrecher, M. Prabhu, Y. Lahini, J. Mower, D. Bunandar, C. Chen, F. N. C. Wong, T. Baehr-Jones, M. Hochberg, S. Lloyd, and D. Englund, Quantum transport simulations in a programmable nanophotonic processor, *Nat. Photonics* **11**, 447 (2017).
- [38] C. Sparrow, E. Martín-López, N. Maraviglia, A. Neville, C. Harrold, J. Carolan, Y. N. Joglekar, T. Hashimoto, N. Matsuda, J. L. O'Brien, D. P. Tew, and A. Laing, Simulating the vibrational quantum dynamics of molecules using photonics, *Nature* **557**, 660 (2018).
- [39] J. Carolan, C. Harrold, C. Sparrow, E. Martín-López, N. J. Russell, J. W. Silverstone, P. J. Shadbolt, N. Matsuda, M.

- Oguma, M. Itoh, G. D. Marshall, M. G. Thompson, J. C. F. Matthews, T. Hashimoto, J. L. O'Brien, and A. Laing, Universal linear optics, *Science* **349**, 711 (2015).
- [40] H. Tang, C. Di Franco, Z. Y. Shi, T. S. He, Z. Feng, J. Gao, Z. M. Li, Z. Q. Jiao, T. Y. Wang, M. S. Kim, and X. M. Jin, Experimental quantum fast hitting on hexagonal graphs, *Nat. Photonics* **12**, 754 (2018).
- [41] A. Crespi, R. Osellame, R. Ramponi, D. J. Brod, E. F. Galvao, N. Spagnolo, C. Vitelli, E. Maiorino, P. Mataloni, and F. Sciarrino, Integrated multimode interferometers with arbitrary designs for photonic boson sampling, *Nat. Photonics* **7**, 545 (2013).
- [42] Z. Chaboyer, T. Meany, L. G. Helt, M. J. Withford, and M. J. Steel, Tunable quantum interference in a 3D integrated circuit, *Sci. Rep.* **5**, 9601 (2015).
- [43] Z. Feng, B. H. Wu, Y. X. Zhao, J. Gao, L. F. Qiao, A. L. Yang, X. F. Lin, and X. M. Jin, Invisibility cloak printed on a photonic chip, *Sci. Rep.* **6**, 28527 (2016).
- [44] A. Szameit, F. Dreisow, T. Pertsch, S. Nolte, and A. Trnnermann, Control of directional evanescent coupling in fs laser written waveguides, *Opt. Express* **15**, 1579 (2007).
- [45] M. Lebugle, M. Gräfe, R. Heilmann, A. Perez-Leija, S. Nolte, and A. Szameit, Experimental observation of N00N state Bloch oscillations, *Nat. Commun.* **6**, 8273 (2015).